JACS
JOURNAL OF THE AMERICAN CHEMICAL SOCIETY
pubs.acs.org/JACS
Article

Nature-Inspired Photocatalytic Azo Bond Cleavage with Red Light

Zijian Zhao, Jili Li, Wei Yuan, Dajiao Cheng, Suze Ma, Ye-Fei Li, Zhang-Jie Shi, and Ke Hu*

Cite This: J. Am. Chem. Soc. 2024, 146, 1364−1373
Read Online
ACCESS | Metrics & More | Article Recommendations | Supporting Information

ABSTRACT: The emerging field of photoredox catalysis in mammalian cells enables spatiotemporal regulation of a wealth of biological processes. However, the selective cleavage of stable covalent bonds driven by low-energy visible light remains a great challenge. Herein, we report that red light excitation of a commercially available dye, abbreviated **NMB**$^+$, leads to catalytic cleavage of stable azo bonds in both aqueous solutions and hypoxic cells and hence a means to photodeliver drugs or functional molecules. Detailed mechanistic studies reveal that azo bond cleavage is triggered by a previously unknown consecutive two-photon process. The first photon generates a triplet excited state, ^{3}**NMB**$^{+}$*, that is reductively quenched by an electron donor to generate a protonated **NMBH**$^{\bullet+}$. The **NMBH**$^{\bullet+}$ undergoes a disproportionation reaction that yields the initial **NMB**$^+$ and two-electron-reduced NMBH (i.e., leuco-NMB, abbreviated as **LNMB**). Interestingly, **LNMB** forms a charge transfer complex with all four azo substrates that possess an intense absorption band in the red region. A second red photon induces electron transfer from **LNMB** to the azo substrate, resulting in azo bond cleavage. The charge transfer complex mediated two-photon catalytic mechanism reported herein is reminiscent of the flavin-dependent natural photoenzyme that catalyzes bond cleavage reactions with high-energy photons. The red-light-driven photocatalytic strategy offers a new approach to bioorthogonal azo bond cleavage for photodelivery of drugs or functional molecules.

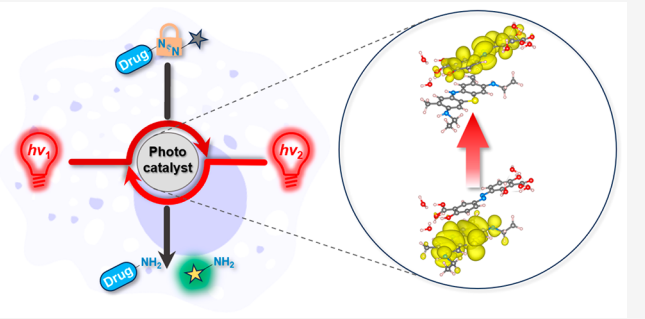

INTRODUCTION

Flavin-dependent enzymes are versatile and important biocatalysts.[1−3] They participate in numerous natural transformations, including glucose oxidation[4,5] and quinone[6]/nitro[7]/azo[8] reduction. The cleavage of azo bonds catalyzed by flavin-dependent azoreductase has been essential in targeted prodrug activation and hypoxic microenvironment detection in tumors and colons.[9−13] Harnessing the energy of light to mimic the natural azoreductase for the cleavage of azo bonds holds great promise to regulate diverse biological processes[14] such as prodrug activation,[15] aptamer/antibody recognition,[16] and gene silencing[17] in mammalian cells. However, the nitrogen−nitrogen double bond has a bond energy of 418 kJ/mol.[18] The cleavage of the first nitrogen−nitrogen bond is approximately half (209 kJ/mol). Therefore, a single photon energy less than 2.2 eV would be insufficient to initiate azo bond cleavage. That energy corresponds to a photon wavelength shorter than 563 nm. The use of low-energy photons with wavelengths in the biological windows (650−900 nm and 1000−1700 nm)[19,20] to drive energy-demanding azo bond cleavage in biological environments remains a great challenge.

The natural flavin-dependent DNA photolyase offers an excellent example of breaking energy-demanding C−C bonds for repairing photodamaged DNA.[21] Nature's strategy is to accumulate multiple photon energies through consecutive photon excitation to achieve a potent excited state for energy-demanding redox chemistry. As shown in Scheme 1, the inactive semireduced radical FADH$^\bullet$ was first reduced to FADH$^-$ through a visible photon.[22] FADH$^-$ was then excited to FADH$^-$* by the second UV photon to accomplish the cleavage of the thermodynamically stable cyclobutene ring.[23] Nonetheless, high-energy visible and UV photons are still required.

In the study reported herein, we discovered that both commercially available methylene blue (**MB**$^+$) and a derivative, new methylene blue (**NMB**$^+$), enable selective and efficient azo bond cleavage through photocatalytic reduction, specifically utilizing red light. The photocatalytic turnover frequency (TOF) for azo bond cleavage is on par with natural azoreductase, with a turnover number (TON) over 6. Intriguingly, the application of intracellular photocatalysis showcases the simultaneous reductive activation of a prodrug and a fluorescent probe that were initially linked by the azo bond. Detailed mechanistic study reveals a fascinating consecutive two-photon mechanism in which a key red-light-absorbing charge transfer complex formed between **LNMB** and

Received: September 7, 2023
Revised: November 23, 2023
Accepted: November 27, 2023
Published: December 11, 2023

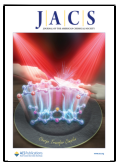

https://doi.org/10.1021/jacs.3c09837
J. Am. Chem. Soc. 2024, 146, 1364−1373

Scheme 1. Photocatalytic C−C Bond Cleavage by Flavin-Dependent Natural DNA Photolyase and Nature-Inspired Photocatalytic Azo Bond Cleavage with Red Light in Mammalian Cells in This Work

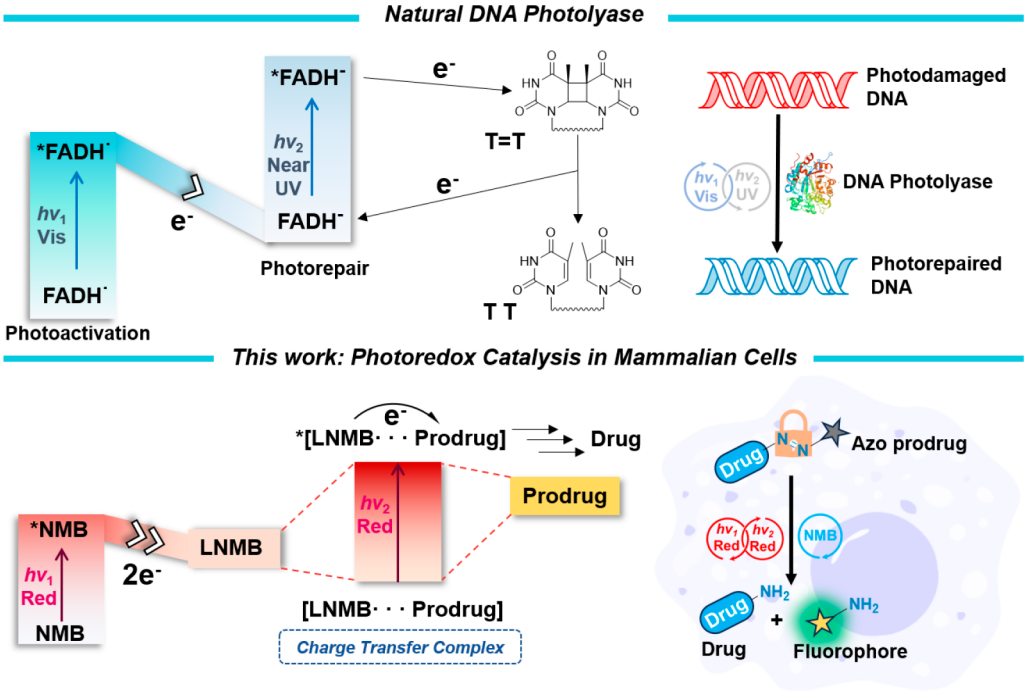

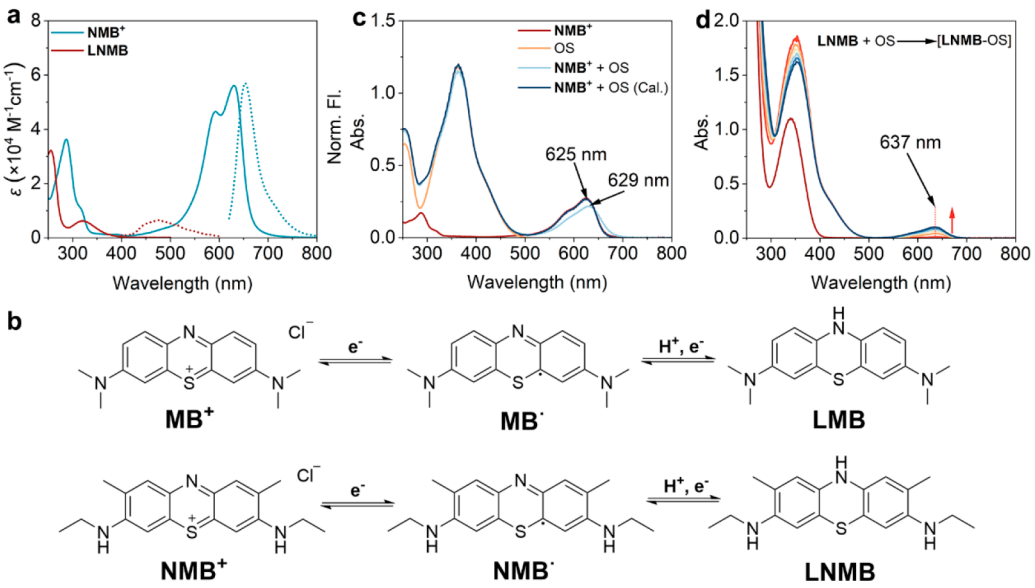

Figure 1. Ground state UV−vis characterizations of **NMB**$^+$ and its ground state ionic associations with OS. (a) UV−vis absorption and fluorescence spectra of **NMB**$^+$ (λ_{ex} = 610 nm) and **LNMB** (λ_{ex} = 320 nm) in water. (b) Stepwise structural changes of **MB**$^+$[Cl$^-$] and **NMB**$^+$[Cl$^-$] upon reduction. (c) Absorption spectra of **NMB**$^+$ (5 μM), OS (50 μM), and their solution mixture; the dark blue line is the calculated spectrum from the sum of **NMB**$^+$ and OS. (d) Absorption spectral changes of the mixture of **LNMB** (5 μM) and OS (50 μM) under an inert atmosphere within 10 min.

the azo substrate was identified. This charge transfer complex-mediated low-energy photon accumulation mechanism is reminiscent of flavin-dependent natural photoenzymes but is also significantly different in terms of extending the photoexcitation wavelength to the red region.

RESULTS

Photophysical and Redox Properties of NMB$^+$. **NMB**$^+$ has a strong visible absorption band in the red region (550−700 nm) due to the n−π* transition associated with the C=S$^+$ chromophore group in the phenothiazinium scaffold. In water, **NMB**$^+$ displays its absorption maximum at 630 nm (ε_{max} = 56 174 M^{-1} cm^{-1}) with a shoulder peak at 593 nm, which arises from the dimer in the aqueous environment (Figure 1a and Figure S1).[24] Additionally, **NMB**$^+$ shows red to near-infrared fluorescence with the emission peak at 653 nm.

Cyclic voltammetry (CV) analysis of **NMB**$^+$ reveals reversible two-electron reduction peaks ($E_{1/2}$ = −0.10 V vs NHE) and an irreversible oxidation peak (E_p = 1.54 V vs NHE) (Figure S2). These CV data suggest that **NMB**$^+$ undergoes a single electron transfer to form semireduced **NMB**$^+$ (**NMB**$^{\bullet}$) and then further

https://doi.org/10.1021/jacs.3c09837
J. Am. Chem. Soc. 2024, 146, 1364−1373

gets fully reduced to leuco-**NMB**$^+$ (**LNMB**) (Figure 1b). The CV profile of **NMB**$^+$ closely resembles that of **MB**$^+$. The UV−vis absorption spectrum of **LNMB**, obtained through chemical reduction with stoichiometric $Na_2S_2O_4$, shows no absorption in the visible region, rendering it colorless. It displays an absorption maxima at 321 nm and an emission maxima at 476 nm. Additional photophysical properties of **NMB**$^+$ and **MB**$^+$ are summarized in Table S1.

To evaluate the photoenzyme-like property of **NMB**$^+$, the anionic azo prodrug olsalazine (OS) was selected as the model substrate.[25] The absorption spectra of cationic **NMB**$^+$ show a bathochromic shift upon the addition of OS in pH = 3.7 acetic acid−acetate buffer solution, attributed to ionic association (Figure 1c).[26] On the other hand, colorless **LNMB**, produced through photoreduction in the presence of the sacrificial electron donor nicotinamide adenine dinucleotide (NADH) (Figure S3), generates a new absorption band in the red region (637 nm) upon the addition of OS under an Ar atmosphere (Figure 1d). This absorption band persists even upon the addition of excess $Na_2S_2O_4$ as the chemical reductant (Figure S4a). When the atmosphere is switched from Ar to air, the new absorption band at 637 nm gradually blue-shifts to 629 nm (Figure S4b). Notably, **MB**$^+$ also displays similar spectral changes to OS (Figures S5 and S6).

The ground state association between **LNMB** and the OS was explored using proton nuclear magnetic resonance (^{1}H NMR) and UV−vis absorption spectra. Incrementally increasing the ratio of **LNMB** to OS in D_2O (from 1:8 to 1:0.5) led to a discernible downfield shift (0.1 ppm) of the protons on the aromatic rings of the OS, indicative of ground state association. To elucidate the specific binding mode of **LNMB** with OS, we constructed a Job plot through the titration of OS to **LNMB**. The most pronounced change in absorbance within the newly emerged absorption band occurred at a mole fraction of approximately 0.5. This suggests a 1:1 binding mode be the most likely between the two molecules (Figure 2a). Furthermore, we determined the binding constant (K_a) of **LNMB** with OS by observing the changes in absorbance in the red region following the incremental addition of OS to **LNMB** (Figure 2b). Using a modified Benisi−Hildebrand analysis,[27] we calculated a K_a value of 2.4×10^4 M^{-1} for **LNMB**. Notably, **LMB** displayed a similar binding mode to OS but with a higher K_a value of 3.3×10^4 M^{-1} (Figures S7 and S8). These results collectively elucidate the ground state interaction between the photocatalysts and the azo prodrug.

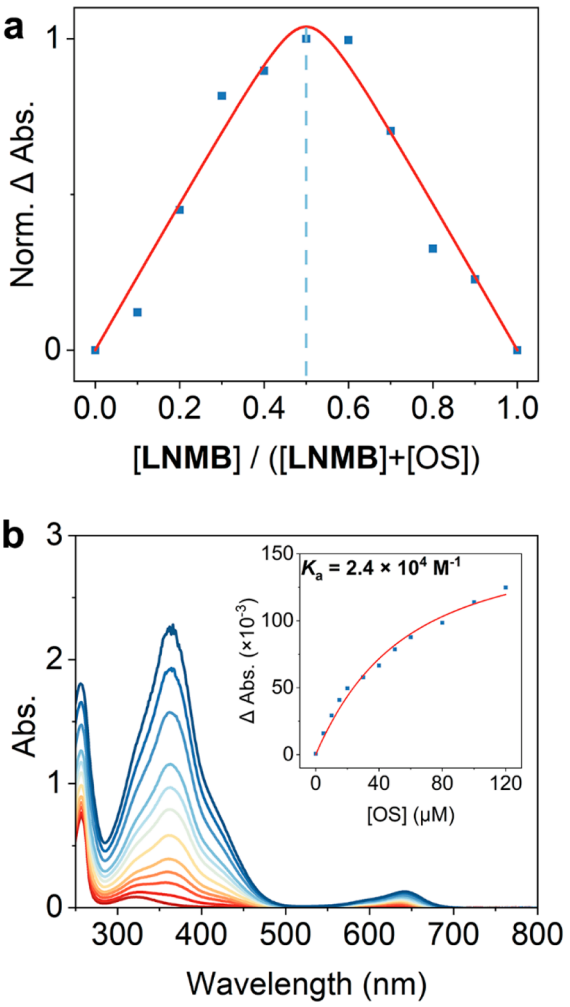

Figure 2. Ground state association of **LNMB** with OS. (a) Job plot for **LNMB** with OS by monitoring the maximum change of absorbance at 637 nm. (b) UV−vis absorption spectra of **LNMB** (20 μM) upon titration of OS. The inset shows the absorbance change at 637 nm with a modified Benisi−Hildebrand analysis.

Photocatalytic Azo Bond Cleavage. We selected four azo prodrugs for our study: olsalazine (OS), balsalazide (BS), sulfasalazine (SS), and SA-azo-C, where SA represents salicylic acid and C is coumarin (Figure 3a). The first three prodrugs are FDA-approved drugs.[25] Notably, OS, BS, and SS can be activated by the azoreductase from anaerobic bacteria in the colon,[28] releasing the active drug mesalazine (MS). Besides MS, SA-azo-C also releases the fluorescent probe coumarin 120 (C) upon reductive cleavage of the azo bond. All azo prodrug substrates show n−π^* transition bands in the visible light region (400−500 nm), characteristic of thermodynamically stable *trans*-photoisomers (Figure S11). Due to fast photochemical isomerization and rotation-mediated nonradiative decay of the singlet excited state,[29] the fluorescence of these azo prodrugs is entirely quenched, in contrast to the highly fluorescent coumarin (Figure S12). CV studies indicate that all azo prodrugs have irreversible 4e$^-$, 4H$^+$ cathodic peaks with E_p ranging from −0.57 to −0.85 V vs NHE,[30] suggesting that their reduction demands substantial energy and directly yields the fully reduced aromatic amine, i.e., the drug MS (Figure S13).

To activate the azo prodrugs, we employed a photocatalyst (PC), either **NMB**$^+$ or **MB**$^+$, and NADH as the electron donor in a 0.2 M pH 3.7 acetic acid−acetate buffer solution. The solution was illuminated with a 655 nm laser (400 mW/cm^2). **NMB**$^+$ demonstrated remarkable photocatalytic efficiency in activating the azo prodrugs within 1 h under standard reaction conditions (Table 1 and Table S2). Among the prodrugs, OS showed the highest photocatalytic conversion yield, approaching unity. Notably, both **MB**$^+$ and **NMB**$^+$ displayed TOFs in the range 10−140 h^{-1} across the azo prodrug series (TON > 6). **NMB**$^+$ had slightly better photocatalytic performance compared to **MB**$^+$ within the same order of magnitude. In some cases, they were superior to natural flavin-dependent azoreductase in terms of the TOF (Figure S15). The photocatalytic efficiency could be further improved with higher laser power and lower pH values, as observed with **NMB**$^+$ and OS (Figures S16 and S17).

HPLC analysis was employed to monitor potential side reactions during the photocatalytic activation of the OS. The result revealed the formation of MS as the sole product (Figure 3b). This observation is consistent with nearly quantitative azo

https://doi.org/10.1021/jacs.3c09837
J. Am. Chem. Soc. 2024, 146, 1364−1373

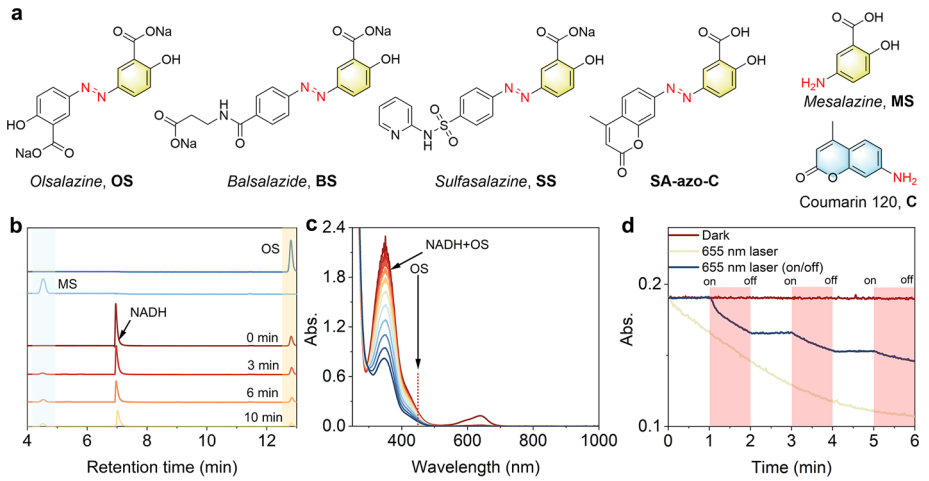

Figure 3. Photocatalytic azo prodrug activation. (a) Molecular structures of azo prodrugs, MS, and coumarin 120. (b) HPLC analysis. (c) Absorption spectral changes upon photocatalytic OS activation under standard reaction conditions. (d) Time-resolved photocatalytic OS activation kinetic traces monitored at 450 nm by on−off switching of the external 655 nm laser.

Table 1. Photocatalytic Azo Prodrug Activation

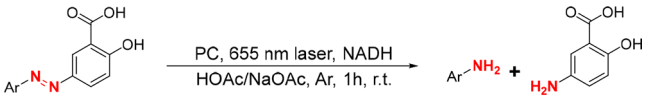

PC	prodrug	TOF (h^{-1})	conversion (%)	yield (%)
NMB$^+$	OS	143	95.8	88.5
	BS	41	93.3	85.7
	SS	31	66.0	64.7
	SA-azo-C	39	88.8	80.9

bond cleavage and release of the active drug. Additionally, changes in the UV−vis absorption spectra during the photoactivation of OS provided more insight (Figure 3c). Before irradiation, NADH and OS displayed characteristic absorption peaks in the UV region. The absorption in the blue region (400−500 nm) belonged solely to OS, and the red region (550−700 nm) belonged to **NMB**$^+$. During irradiation, the absorption peak in the red rapidly bleached within 30 s, concurrently with a swift decrease of absorption in the UV and blue regions. These spectral changes were attributed to the reductive cleavage of the OS azo bond and oxidation of NADH. The absorbance kinetic trace at 450 nm, where only OS absorbed appreciably, showed a sensitive response to 655 nm light on−off cycles. The absorption decreased during light exposure but remained unchanged during light-off periods (Figure 3d), clearly indicating the indispensability of light for the reductive cleavage of the OS azo bond.

The control experiments revealed the essential role of several factors, including the PC, light, electron donor (NADH), and inert atmosphere, for the successful photocatalytic activation of azo prodrugs, as outlined in Table S3. Additionally, a series of red-light-absorbing dyes (Figure 4a,b) were selected for comparison in photocatalytic prodrug activation. Among these dyes, BB3 and BB12 share a phenoxazine scaffold. These two dyes displayed negligible photocatalytic activity. This lack of activity is likely because of short excited state lifetimes of these dyes typically on the order of several nanoseconds so that NADH at low concentration (200 μM) would be inefficient to quench the excited state PC.[31] ZnPC and Ce6 are traditional triplet photosensitizers with phthalocyanine/porphyrin scaffolds. They also demonstrated negligible photocatalytic activity although having a long-lived triplet excited state. This is likely due to their insufficiently low excited state redox potential for photoreduction. Only GS and thionin, characterized by the phenothiazine scaffold and a cationic D−A resonance structure, showed measurable photocatalytic activities toward OS. Comparing their molecular structure to that of **NMB**$^+$ and **MB**$^+$, we can deduce that the presence of a reversible two-electron/one-proton phenothiazine scaffold with a heavy atom-enhanced triplet excited state is necessary for the molecular PC in photocatalytic azo prodrug activation, especially at low concentrations of the electron donor and the substrate (μM range). These mild conditions offer unique advantages for photocatalytic azo prodrug activation within cellular microenvironments.

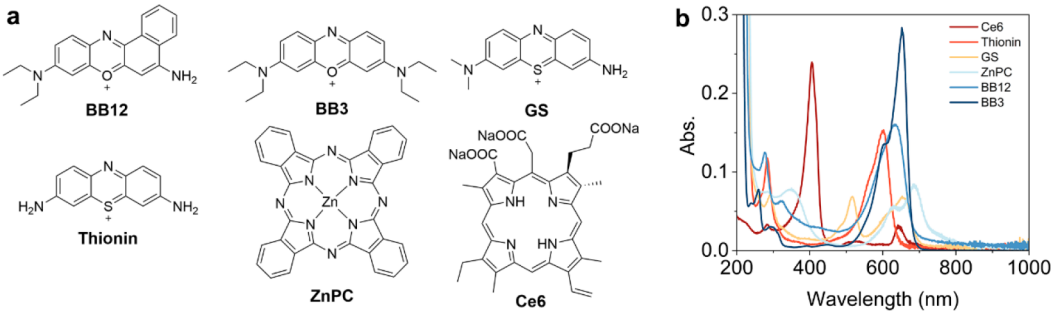

Figure 4. Red-light-absorbing PCs in control experiments. (a) Molecular structures of control PCs and (b) absorption spectra of control PCs in water.

https://doi.org/10.1021/jacs.3c09837
J. Am. Chem. Soc. 2024, 146, 1364−1373

Transient Absorption Spectroscopy. Nanosecond transient absorption spectroscopy was employed to investigate the kinetics of the excited state and the semireduced state of **NMB**$^+$. Figure 5a displays the absorption difference spectra of the triplet excited states of **NMB**$^+$ after 640 nm pulsed-laser excitation in pH 3.7 acetic acid−acetate buffer solution under an inert atmosphere. It revealed two excited state absorption (ESA) bands at 330−510 nm and 660−800 nm, with peaks at 370 and 700 nm, as well as a ground state bleach (GSB) in the range of 510−660 nm. The triplet excited state lifetime of **NMB**$^+$ was determined to be 5.0 μs (Figure S18). Similarly, the **MB**$^+$ excited state displayed similar transient absorption features and a triplet excited state lifetime of 4.2 μs (Figure S18).

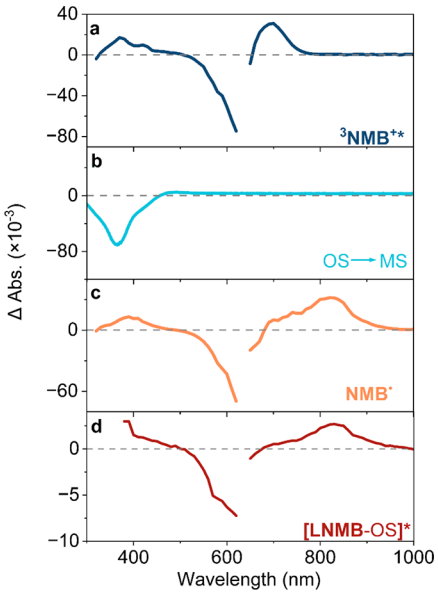

Figure 5. Nanosecond transient absorption spectra. (a) Absorption difference spectrum of **NMB**$^+$ (5 μM) in acetic acid−acetate buffer solution at 50 ns time delay after pulsed laser excitation. (b) Absorption difference spectrum of OS (100 μM) in 0.1 M $Na_2S_2O_4$ aqueous solution at an applied bias of −1.2 V vs NHE. (c) Absorption difference spectrum of **NMB**$^+$ (5 μM) in HQ (5 mM) aqueous solution at 30 μs time delay after pulsed laser excitation. (d) Absorption difference spectrum of **NMB**$^+$ (5 μM) in the presence of $Na_2S_2O_4$ (10 μM) and OS (50 μM) in acetic acid−acetate buffer solution at 10 μs time delay after pulsed laser excitation (λ_{ex} = 640 nm).

$$\mathbf{NMB}^{+*} + \mathrm{HQ} \rightarrow \mathbf{NMB}^{\bullet} + \mathrm{HQ}^{+} \quad (1)$$

$$\mathbf{NMB}^{\bullet} + \mathrm{H}^{+} \rightarrow \mathbf{NMBH}^{\bullet+} \quad (2)$$

$$2\mathbf{NMBH}^{\bullet+} \rightarrow \mathbf{NMB}^{+} + \mathbf{LNMB} + \mathrm{H}^{+} \quad (3)$$

Reductive quenching of ^{3}**NMB**$^{+*}$ in the presence of excess hydroquinone (HQ) as the electron donor generated the transient absorption spectra of the semireduced **NMB**$^•$ right after the laser pulse (eq 1), as shown in Figure 5c and Figure S19. The characteristic absorption bands of **NMB**$^•$ were observed in the 330−550 nm range and the near-infrared (NIR) region (700−1000 nm). **NMB**$^•$ would then accept a proton and generate **NMB**$^+$ and **LNMB** through disproportionation (eqs 2 and 3). The bimolecular disproportionation was found to be diffusion-controlled with a fitted rate constant $k_{disp} = 6.6 \times 10^9$ M^{-1} s^{-1} (Figure S20).

$$[\mathbf{LNMB}\text{-OS}]^{*} \rightarrow \mathbf{NMB}^{\bullet} + \mathrm{OS}^{-} + \mathrm{H}^{+} \quad (4)$$

When OS was present in **NMB**$^+$ solution, no photoinduced electron transfer (PET) was observed between ^{3}**NMB**$^{+*}$ and OS despite a slight decrease in the triplet excited state lifetimes (Figure S21). Then, the [**LNMB**-OS] ground state was obtained by the addition of excess chemical reductant $Na_2S_2O_4$ to the solution of 1 to 10 molar ratio of **NMB**$^+$ and OS. After 640 nm pulsed laser excitation into the newly formed [**LNMB**-OS] absorption band, a relatively weak transient absorption spectrum appeared that matched the spectrum of **NMB**$^•$, as illustrated in

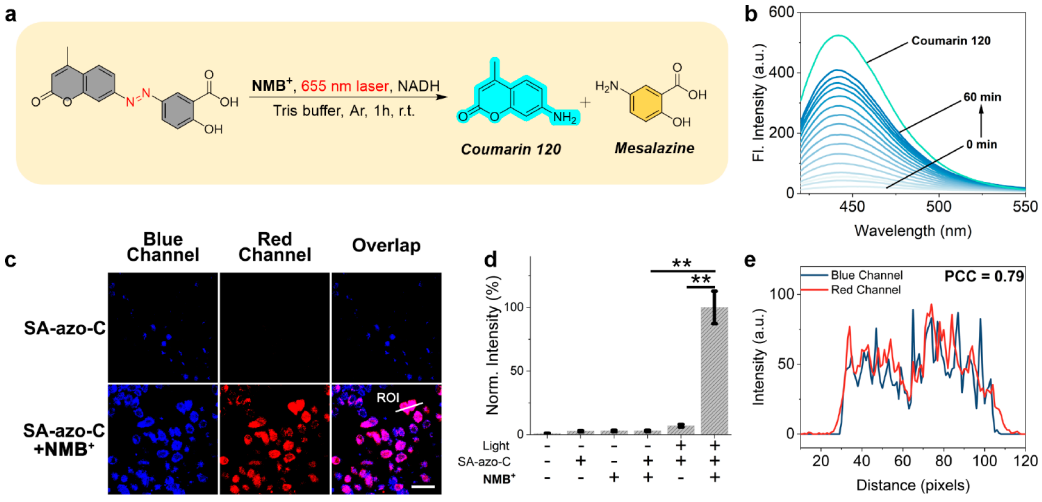

Figure 6. Photocatalytic SA-azo-C activation in solution and hypoxic cells. (a) Photocatalytic SA-azo-C activation in pH = 6.8 Tris buffer solution and (b) fluorescence spectral changes of the ongoing photocatalytic reaction shown in (a) within 1 h (λ_{ex} = 405 nm). (c) Confocal microscopic images of hypoxic HeLa cells under the indicated conditions. Images in the left column (blue channel, λ_{ex} = 405 nm, λ_{em} = 470 ± 50 nm) represent blue fluorescence of decaged coumarin 120; images in the middle column (red channel, λ_{ex} = 633 nm, λ_{em} = 690 ± 50 nm) represent red fluorescence of **NMB**$^+$; images in the right column are overlaps of the above two channels. Scale bar: 50 μm. (d) Normalized fluorescence intensity collected from the blue fluorescence channel. Data are represented as mean ± SD (n = 3 independent samples). **p < 0.001. (e) Colocalization between the blue and red fluorescence channel in the region of interest (ROI).

https://doi.org/10.1021/jacs.3c09837
J. Am. Chem. Soc. 2024, 146, 1364−1373

Figure 5c and d. The characteristic absorption band in the NIR region (700−1000 nm) suggested that the transient absorption signal originated from **NMB**$^{\bullet}$, not ^{3}**NMB**$^{+}$*. This indicates that red-light excitation of the charge transfer complex yields **NMB**$^{\bullet}$ and OS^{-} as the charge-separated state (eq 4). The charge-separated state returns to the original charge transfer complex within hundreds of microseconds (Figure S22). Similar transient absorption spectra were obtained when **LNMB** was replaced by **LMB** (Figure S23).

Photocatalytic Azo Prodrug Activation in Hypoxic Cells. The application of molecular photoactivated agents for cancer photodynamic therapy is severely restricted in hypoxic microenvironments.[32] As an alternative approach, photocatalytic therapy has garnered significant attention in recent years due to its oxygen-independent characteristics.[33−35] One example involves the photoactivation of prodrugs and the disruption of electron transport with NADH depletion.[36,37] Building upon the demonstrated efficient azo bond cleavage with red light, our objective was to visualize the activation of photocatalytic azo prodrugs in living hypoxic cells. To achieve this, the nonfluorescent azo-caged SA-azo-C was selected as the model prodrug and **NMB**$^{+}$ as the model PC. Notably, **NMB**$^{+}$ and SA-azo-C showed suitable biocompatibility based on the cytotoxicity test (Figures S24 and S25). Before proceeding with *in vitro* experiments, we first monitored the photocatalytic activation of SA-azo-C using fluorescence turn-on under simulated cellular pH environments (pH = 6.8 Tris buffer solution). As shown in Figure 6a,b, laser irradiation (655 nm) of a solution containing SA-azo-C (50 μM), **NMB**$^{+}$ (50 μM), and NADH (200 μM) under an inert atmosphere led to a gradual increase in fluorescence, consistent with the photouncaging of fluorescent coumarin 120. The yield of activated MS, calculated from the fluorescent intensity of an equivalent amount of coumarin 120, was measured to be 46.9% within 1 h.

NMB^{+} was selected as the model PC for *in vitro* photocatalytic azo prodrug activation under hypoxia. As shown in Figure S26, SA-azo-C has the highest binding constant with **LNMB** and did show the highest activation efficiency. However, there is no obvious relationship between the binding constant and activation in the other three azo prodrugs. To visualize the photocatalytic process, confocal laser scanning microscopy (CLSM) was employed to monitor the fluorescence turn-on from the caged prodrug SA-azo-C. HeLa cells were incubated with **NMB**$^{+}$ and SA-azo-C, followed by irradiation with a 655 nm laser (20 min, 20 mW/cm^2) under hypoxic conditions (0.1% O_2). Figure 6c−e demonstrate that decaged coumarin 120 displayed significant blue fluorescence, which colocalized with the red fluorescence of **NMB**$^{+}$ with a high Pearson colocalization coefficient (PCC) of 0.79. The substantial PCC indicates considerable photocatalytic activation of SA-azo-C in hypoxic cells; that is to say, the red fluorescence of **NMB**$^{+}$ and blue fluorescence of coumarin 120 overlapped most significantly after photoinduced electron transfer from **LNMB** to OS. It is worth noting that the observed weak blue fluorescence in the absence of **NMB**$^{+}$ can be attributed to the presence of endogenously overexpressed azoreductase in hypoxic cancer cells as previously reported.[9,28,38] The Supporting Information (Figures S27−S29) provides the results of the control experiments. The CLSM data revealed excellent photocatalytic SA-azo-C activation by **NMB**$^{+}$, effectively depleting cellular electron donors in hypoxic cells.

DISCUSSION

Practical biomedical applications involving photochemistry generally require the use of low-energy photons in the so-called biological windows (650−900 nm and 1000−1700 nm).[19,20] The need for both low-energy light and bond cleavage reactivity provides a conundrum, as the energy of the absorbed photon sets a thermodynamic limit as to what type of bonds can be cleaved. The discovery of red light reactivity in azo bond cleavage, despite the ostensible mismatch of photon and bond energy, requires a thorough investigation into the underlying mechanism. In the discussion below, emphasis is placed on the elucidation of the proposed two-photon catalytic mechanism governing azo bond cleavage, along with its profound implications for the broader domain of bioorthogonal bond cleavage reactions.

Two-Photon Catalytic Mechanism. As a classical photocatalyst or photosensitizer, **MB**$^{+}$ and its derivatives have garnered significant attention for their photochemical properties and applications.[37,39−41] The photocatalytic mechanism of **MB**$^{+}$ predominantly involves single-electron transfer (SET). In most scenarios, **MB**$^{+}$ acts as a potent photooxidant (E^{*}_{red} = +1.42 V vs NHE).[39] The excited state redox potential for oxidative quenching (E^{*}_{ox} = −0.12 V vs NHE) is considerably less negative and unfavorable for challenging bond cleavage, such as the stable azo bond. The results shown above in which **NMB**$^{+}$ or **MB**$^{+}$ could readily catalyze the cleavage of azo bonds in the presence of NADH and red light are quite surprising. The question is why photocatalysis could indeed occur.

To investigate the mechanism, we selected OS as the model substrate with an irreversible redox potential for reduction at E_{red} = −0.85 V vs NHE and a quasi-reversible redox potential for the first oxidation at E_{ox} = +0.84 V vs NHE (Figure S14). **NMB**$^{+}$ was chosen as the model PC for the subsequent discussion. The steady and transient absorption spectra (Figure 1d and Figure S30) clearly indicate that neither **LNMB** nor **NMB**$^{\bullet}$ could reduce OS. Direct azo bond cleavage through triplet excited state OS is also highly unlikely, as free energy from ^{3}**NMB**$^{+}$* is too low (1.73 eV)[42] to do the energy transfer.

We propose a multiphoton-driven catalytic cycle for the photocatalytic activation of azo bond-containing prodrugs. Two potential reaction pathways emerge in the multiphoton excitation photoredox catalysis: (I) consecutive excitation leading to doublet excited states via **NMB**$^{\bullet}$; (II) consecutive excitation of the charge transfer complex formed between the prodrug and **LNMB**. Each hypothesis is further explored in the discussion below. Note that the first hypothesis relating to doublet excited states for a number of organic photocatalysts was often invoked in some recent studies on organic photoredox catalysis.[43−47]

One of the drawbacks of the doublet excited states for photocatalysis is their extremely short lifetimes ($\tau \sim$ 10 ps to 5 ns),[43,48] which limits diffusional encounters occurring at low concentrations.[47,49] Due to the rapid disproportionation reaction of **NMB**$^{\bullet}$ (k_{disp} = 6.6 × 10^{9} M^{-1} s^{-1}), a negligible amount of **NMB**$^{\bullet}$ would be present in the steady state to be photoexcited again. The low micromolar concentration of prodrugs precludes the SET from the doublet excited state of **NMB**$^{\bullet}$. Therefore, we believe that the doublet excited state pathway via **NMB**$^{\bullet}$ is less likely.

Drawing inspiration from photobiocatalytic organic synthesis by flavin-dependent enzymes,[50−52] we think the photocatalytic mechanism based on hypothesis (II) shown in Scheme 2 is more

https://doi.org/10.1021/jacs.3c09837
J. Am. Chem. Soc. 2024, 146, 1364−1373

Scheme 2. Energy Diagram and Proposed Photoredox Catalytic Cycle

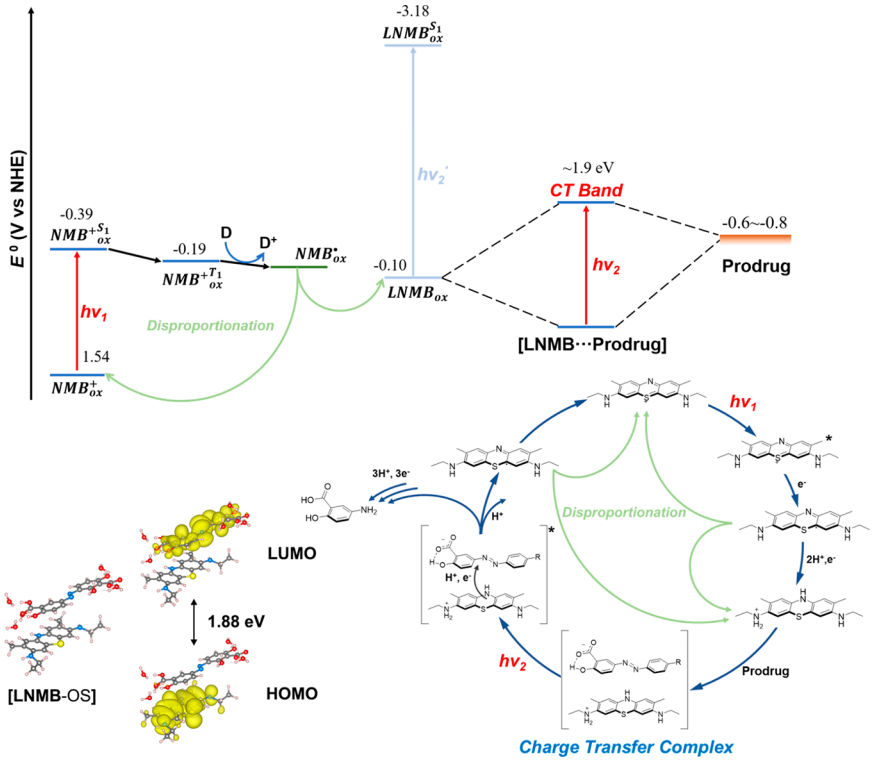

likely. In this scenario, colorless **LNMB** forms a red-absorbing charge transfer complex with the azo prodrug. Excitation of this new charge transfer (CT) band activates azo prodrugs through photoreduction within the charge transfer complex. Subsequently, **NMB**$^{\bullet}$ recovers to **NMB**$^{+}$ and **LNMB** via disproportionation, thereby completing the catalytic cycle.

The linchpin in this mechanism is the charge transfer complex formed between **LNMB** and the azo prodrugs. Given the pK_a of analogue **LMB** (5.8)[53] and salicylic acid (2.9)[54] on OS, the ion-paired charge transfer complex (cationic electron-rich **LNMB** and anionic electron-poor azo prodrugs) could be formed in a mildly acidic solution of which the pH is between 2.9 and 5.8. Loss of ionic association in the charge transfer complex beyond the pH range aligns with the observed pH-dependent TOF of photocatalytic azo prodrug activation, where the TOF decreased sharply with an increase in pH (Figure S17). ^{1}H NMR titration experiments corroborate with the ionic association between **LNMB** and OS. Upon the titration of cationic **LNMB**, the proton resonance signal of anionic OS displays a downfield shift due to a reduced shielding effect. Moreover, the emergence of a new absorption band in the red, as observed in Figure 1d and Figure S6, substantiates CT between **LNMB** and OS within the charge transfer complex.

First-principles calculations were performed to elucidate the atomic configuration and energy gaps of the charge transfer complexes for the [**LNMB**-OS] and [**LMB**-OS] ground states. Using the stochastic surface walking (SSW) global optimization method combined with the neural network (NN) potential energy surface,[55,56] the global minimum and configuration energy spectra of the [**LNMB**-OS] are illustrated in the lower left of Scheme 2 and Figures S31 and S32. In the [**LNMB**-OS] charge transfer complex, both **LNMB** and OS entities adopt an approximately planar conformation due to the rigidity of the benzene group. The computed energy gap of the [**LNMB**-OS] is 1.88 eV, where the HOMO and LUMO are entirely localized on **LNMB** and OS, respectively, in the ion-paired [**LNMB**-OS] ground state, indicating the supramolecular charge transfer character in the charge transfer complex. Notably, the hydrogen bonding between the −NH− group of **LNMB** and the −COOH group of OS may also contribute to the formation of the [**LNMB**-OS]. The density functional theory (DFT) computational result is in excellent agreement with the experimentally observed low-energy absorption peak (637 nm/1.95 eV, Figure 1c) in the UV−vis absorption spectra of [**LNMB**-OS]. Hence, we reasonably believe that the absorption of [**LNMB**-OS] in the red region is originated from the charge transfer from **LNMB** to OS. Notably, **LMB** displayed a similar structural binding mode and charge transfer energy matching compared to **LNMB** according to experimental and computational results (Figures S6, 33 and S34).

The transient absorption spectroscopy study provided incontrovertible evidence of this mechanism. Upon pulsed-laser excitation of the CT absorption band in the red region, the consistent absorption characteristics of **NMB**$^{\bullet}$ clearly showed up in the longer time delay range (10 μs to 2 ms) with consistent recovery rate constants in the red and NIR region (Figure 5d and Figure S22). It was observed that ^{3}**NMB**$^{+}$*, quenched by the OS, showed no absorption beyond 10 μs (Figure S21). This characteristic absorption signal could be attributed to only the charge transfer in the ion-paired charge transfer complex, resulting in the generation of **NMB**$^{\bullet}$ and reduced OS. In light of the aforementioned discussion, the full photoredox catalytic cycle involving charge-transfer-mediated photocatalytic activation of azo prodrugs through two red photons has been established and elucidated.

Implication for Broader Bioorthogonal Bond Cleavage Reactions. The selection of a PC for the photocatalytic reductive cleavage of azo bonds under red light has been

https://doi.org/10.1021/jacs.3c09837
J. Am. Chem. Soc. 2024, 146, 1364−1373

Scheme 3. Existing Bioorthogonal Cleavage Reactions and Azo Bond Based BCR

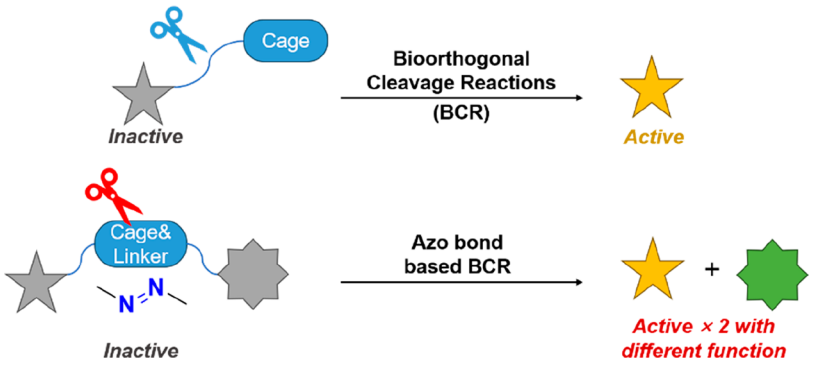

identified as both characteristic and broad, specifically those with a phenothiazine scaffold and cationic D−A resonance structure. More importantly, these series of PCs display negligible photocatalytic activities toward breaking stronger bonds such as the C−C bond. It is of significant interest to develop photocatalytic selective bond cleavage reactions in complex environments based on the developed PCs.

Bioorthogonal cleavage reactions (BCRs) have emerged as powerful tools for reactivating target components caged by protecting groups.[57,58] Among the most reported BCR systems, linker bond cleavage is initiated from the "consumption" of the protecting group. If the bioactive component recovers its bioactivity by light-triggered BCRs, the specific caged type is called "photocaged". Photoactivated chemotherapy (PACT)[59−61] is one of the emerging photocaged methods for treating diseases like cancer in which intracellular oxygen is no longer a necessity. Yet most reported light absorbers applied in PACT are based on noble metal compounds and have limited light absorption in the biological window. The photoreleased chemodrug is also very often limited to only one species.[62,63]

Azo bonds, as unique chemical entities, hold immense promise for serving dual functions as both the linker and protecting group, thereby offering more alternative functional molecules on the other side of the azo bond (Scheme 3). However, despite their potential advantages, photocatalytic cleavage of azo bonds in cells still presents a significant challenge due to their intrinsic high chemical stability. Overcoming this obstacle and achieving efficient bond cleavage selectively in cellular environments is a challenging task. The successful demonstration of releasing both a fluorescent probe and a mesalazine drug from selective azo bond cleavage with red light highlights the innovative photocatalytic strategy to navigate the intricate interplay between chemical reactivity and biological complexity. This achievement not only expands the toolbox of bioorthogonal chemistry but also paves the way for tailoring novel and finely tuned cellular responses through precise control of azo bond cleavage.

CONCLUSION

The potent photoredox reactivity of methylene blue (**MB**$^+$) and its structural analogue new methylene blue (**NMB**$^+$) was shown to cleave the thermodynamically stable azo bonds under red light excitation. Ground state spectroscopic data revealed the ionic association between reduced **NMB**$^+$ (**LNMB**) and azo substrates in 1 to 1 ratio with the association equilibrium constant K_a on the order of 10^3 to 10^5 M^{-1}. DFT indicated that the ionic association resulted in a new charge transfer transition from **LNMB** to an azo substrate with a HOMO−LUMO gap of 1.88 eV, in good agreement with the experimentally observed position of the charge transfer band. The charge transfer complex formed after reductive quenching of **NMB**$^{+}$* enabled its absorption of the second red photon, which led to the reductive cleavage of the azo bond. The consecutive two-photon catalytic strategy circumvents the conundrum in the emerging field of photoredox catalysis in mammalian cells where both low-energy light in the so-called biological windows and stable bond cleavage are needed. The consecutive two-photon absorption mechanism also significantly differs from the direct two-photon absorption where the absorption cross section is rather low. The successful application of red light induced cleavage of azo bonds for photodelivery of drugs and fluorescent probes in mammalian cells signifies a substantial advancement in the field of photocatalytic bioorthogonal cleavage reactions and azo prodrug activation. The advantage of caging two bioactive molecules using azo bonds can be further exploited in the broader bioorthogonal bond cleavage reactions.

ASSOCIATED CONTENT

Supporting Information

The Supporting Information is available free of charge at https://pubs.acs.org/doi/10.1021/jacs.3c09837.

Experimental details, additional spectroscopic and electrochemical characterizations, synthesis of SA-azo-C, transient absorption and kinetics analysis, controlled photocatalytic experiments in cells, and computational methods (PDF)

AUTHOR INFORMATION

Corresponding Author

Ke Hu − *Department of Chemistry, Fudan University, Shanghai 200433, People's Republic of China*; orcid.org/0000-0002-0240-7192; Email: khu@fudan.edu.cn

Authors

Zijian Zhao − *Department of Chemistry, Fudan University, Shanghai 200433, People's Republic of China*

Jili Li − *Department of Chemistry, Fudan University, Shanghai 200433, People's Republic of China*

Wei Yuan − *Shanghai Frontiers Science Research Base of Intelligent Optoelectronics and Perception, Institute of Optoelectronics and Institute of Optoelectronics, Fudan University, Shanghai 200438, People's Republic of China*; orcid.org/0000-0002-2728-6841

Dajiao Cheng − *Department of Chemistry, Fudan University, Shanghai 200433, People's Republic of China*

https://doi.org/10.1021/jacs.3c09837
J. Am. Chem. Soc. 2024, 146, 1364−1373

Suze Ma − *Department of Chemistry, Fudan University, Shanghai 200433, People's Republic of China;* orcid.org/0000-0001-8030-2401
Ye-Fei Li − *Department of Chemistry, Fudan University, Shanghai 200433, People's Republic of China;* orcid.org/0000-0003-4433-7433
Zhang-Jie Shi − *Department of Chemistry, Fudan University, Shanghai 200433, People's Republic of China;* orcid.org/0000-0002-0919-752X

Complete contact information is available at: https://pubs.acs.org/10.1021/jacs.3c09837

Notes

The authors declare no competing financial interest.

■ ACKNOWLEDGMENTS

This study is sponsored by the National Natural Science Foundation of China (22173022) and Natural Science Foundation of Shanghai (21ZR1404400). The authors thank Prof. Gerald J. Meyer from UNC Chapel Hill and Prof. Wenbo Bu from Fudan University for insightful discussions during preparation of the manuscript.

■ REFERENCES

(1) Joosten, V.; van Berkel, W. J. Flavoenzymes. *Curr. Opin. Chem. Biol.* **2007**, *11*, 195−202.
(2) Walsh, C. T.; Wencewicz, T. A. Flavoenzymes: versatile catalysts in biosynthetic pathways. *Nat. Prod. Rep.* **2013**, *30*, 175−200.
(3) Fraaije, M. W.; Mattevi, A. Flavoenzymes: diverse catalysts with recurrent features. *Trends Biochem. Sci.* **2000**, *25*, 126−132.
(4) Mattevi, A. To be or not to be an oxidase: challenging the oxygen reactivity of flavoenzymes. *Trends Biochem. Sci.* **2006**, *31*, 276−283.
(5) Romero, E.; Gomez Castellanos, J. R.; Gadda, G.; Fraaije, M. W.; Mattevi, A. Same Substrate, Many Reactions: Oxygen Activation in Flavoenzymes. *Chem. Rev.* **2018**, *118*, 1742−1769.
(6) Deller, S.; Macheroux, P.; Sollner, S. Flavin-dependent quinone reductases. *Cell. Mol. Life Sci.* **2008**, *65*, 141−160.
(7) Roldan, M. D.; Perez-Reinado, E.; Castillo, F.; Moreno-Vivian, C. Reduction of polynitroaromatic compounds: the bacterial nitroreductases. *FEMS Microbiol. Rev.* **2008**, *32*, 474−500.
(8) Misal, S. A.; Gawai, K. R. Azoreductase: a key player of xenobiotic metabolism. *Bioresour. Bioprocess.* **2018**, *5*, 17.
(9) Liu, J. N.; Bu, W.; Shi, J. Chemical Design and Synthesis of Functionalized Probes for Imaging and Treating Tumor Hypoxia. *Chem. Rev.* **2017**, *117*, 6160−6224.
(10) Hao, D.; Meng, Q.; Jiang, B.; Lu, S.; Xiang, X.; Pei, Q.; Yu, H.; Jing, X.; Xie, Z. Hypoxia-Activated PEGylated Paclitaxel Prodrug Nanoparticles for Potentiated Chemotherapy. *ACS Nano* **2022**, *16*, 14693−14702.
(11) Liu, J.; Prentice, A. W.; Clarkson, G. J.; Woolley, J. M.; Stavros, V. G.; Paterson, M. J.; Sadler, P. J. A Concerted Redox- and Light-Activated Agent for Controlled Multimodal Therapy against Hypoxic Cancer Cells. *Adv. Mater.* **2023**, *35*, No. e2210363.
(12) Guisan-Ceinos, S.; Rivero, R. R.; Romeo-Gella, F.; Simon-Fuente, S.; Gomez-Pastor, S.; Calvo, N.; Orrego, A. H.; Guisan, J. M.; Corral, I.; Sanz-Rodriguez, F.; Ribagorda, M. Turn-on Fluorescent Biosensors for Imaging Hypoxia-like Conditions in Living Cells. *J. Am. Chem. Soc.* **2022**, *144*, 8185−8193.
(13) Zhao, X. B.; Ha, W.; Gao, K.; Shi, Y. P. Precisely Traceable Drug Delivery of Azoreductase-Responsive Prodrug for Colon Targeting via Multimodal Imaging. *Anal. Chem.* **2020**, *92*, 9039−9047.
(14) Cheng, H. B.; Zhang, S.; Qi, J.; Liang, X. J.; Yoon, J. Advances in Application of Azobenzene as a Trigger in Biomedicine: Molecular Design and Spontaneous Assembly. *Adv. Mater.* **2021**, *33*, No. e2007290.
(15) Piao, W.; Hanaoka, K.; Fujisawa, T.; Takeuchi, S.; Komatsu, T.; Ueno, T.; Terai, T.; Tahara, T.; Nagano, T.; Urano, Y. Development of an Azo-Based Photosensitizer Activated under Mild Hypoxia for Photodynamic Therapy. *J. Am. Chem. Soc.* **2017**, *139*, 13713−13719.
(16) Zhou, F.; Fu, T.; Huang, Q.; Kuai, H.; Mo, L.; Liu, H.; Wang, Q.; Peng, Y.; Han, D.; Zhao, Z.; Fang, X.; Tan, W. Hypoxia-Activated PEGylated Conditional Aptamer/Antibody for Cancer Imaging with Improved Specificity. *J. Am. Chem. Soc.* **2019**, *141*, 18421−18427.
(17) Perche, F.; Biswas, S.; Wang, T.; Zhu, L.; Torchilin, V. P. Hypoxia-targeted siRNA delivery. *Angew. Chem., Int. Ed.* **2014**, *53*, 3362−3366.
(18) Luo, Y.-R. *Comprehensive Handbook of Chemical Bond Energies*; CRC Press, 2007.
(19) Weissleder, R. A clearer vision for in vivo imaging. *Nat. Biotechnol.* **2001**, *19*, 316−317.
(20) Smith, A. M.; Mancini, M. C.; Nie, S. Second window for in vivo imaging. *Nat. Nanotechnol.* **2009**, *4*, 710−711.
(21) Brettel, K.; Byrdin, M. Reaction mechanisms of DNA photolyase. *Curr. Opin. Struct. Biol.* **2010**, *20*, 693−701.
(22) Aubert, C.; Vos, M. H.; Mathis, P.; Eker, A. P.; Brettel, K. Intraprotein radical transfer during photoactivation of DNA photolyase. *Nature* **2000**, *405*, 586−590.
(23) Liu, Z.; Tan, C.; Guo, X.; Kao, Y.-T.; Li, J.; Wang, L.; Sancar, A.; Zhong, D. Dynamics and mechanism of cyclobutane pyrimidine dimer repair by DNA photolyase. *Proc. Natl. Acad. Sci. U. S. A.* **2011**, *108*, 14831−14836.
(24) Junqueira, H. C.; Severino, D.; Dias, L. G.; Gugliotti, M. S.; Baptista, M. S. Modulation of methylene blue photochemical properties based on adsorption at aqueous micelle interfaces. *Phys. Chem. Chem. Phys.* **2002**, *4*, 2320−2328.
(25) Sousa, T.; Yadav, V.; Zann, V.; Borde, A.; Abrahamsson, B.; Basit, A. W. On the colonic bacterial metabolism of azo-bonded prodrugsof 5-aminosalicylic acid. *J. Pharm. Sci.* **2014**, *103*, 3171−3175.
(26) Basu, S.; Ghosh, S. K.; Kundu, S.; Nath, S.; Panigrahi, S.; Praharaj, S.; Pal, T. Studies on the ion-association of methylene blue and salicylic acid in neat and mixed binary solvents. *Chem. Phys. Lett.* **2005**, *407*, 493−497.
(27) Ward, W. M.; Farnum, B. H.; Siegler, M.; Meyer, G. J. Chloride ion-pairing with Ru(II) polypyridyl compounds in dichloromethane. *J. Phys. Chem. A* **2013**, *117*, 8883−8894.
(28) Ryan, A. Azoreductases in drug metabolism. *Br. J. Pharmacol.* **2017**, *174*, 2161−2173.
(29) Chevalier, A.; Renard, P. Y.; Romieu, A. Azo-Based Fluorogenic Probes for Biosensing and Bioimaging: Recent Advances and Upcoming Challenges. *Chem.-Asian J.* **2017**, *12*, 2008−2028.
(30) Dmukhailo, A.; Tvorynska, S.; Dubenska, L. Rapid and straightforward electrochemical approach for the determination of the toxic food azo dye tartrazine using sensors based on silver solid amalgam. *J. Electroanal. Chem.* **2023**, *932*, No. 117250.
(31) Martinez, V.; Henary, M. Nile red and nile blue: applications and syntheses of structural analogues. *Chem.—Eur. J.* **2016**, *22*, 13764−13782.
(32) Pham, T. C.; Nguyen, V. N.; Choi, Y.; Lee, S.; Yoon, J. Recent Strategies to Develop Innovative Photosensitizers for Enhanced Photodynamic Therapy. *Chem. Rev.* **2021**, *121*, 13454−13619.
(33) Huang, H.; Banerjee, S.; Qiu, K.; Zhang, P.; Blacque, O.; Malcomson, T.; Paterson, M. J.; Clarkson, G. J.; Staniforth, M.; Stavros, V. G.; Gasser, G.; Chao, H.; Sadler, P. J. Targeted photoredox catalysis in cancer cells. *Nat. Chem.* **2019**, *11*, 1041−1048.
(34) Chen, L.; Jiang, X.; Lv, M.; Wang, X.; Zhao, P.; Zhang, M.; Lv, G.; Wu, J.; Liu, Y.; Yang, Y.; Chen, J.; Bu, W. Reductive-damage-induced intracellular maladaptation for cancer electronic interference therapy. *Chem.* **2022**, *8*, 866−879.
(35) Li, M.; Gebremedhin, K. H.; Ma, D.; Pu, Z.; Xiong, T.; Xu, Y.; Kim, J. S.; Peng, X. Conditionally Activatable Photoredox Catalysis in Living Systems. *J. Am. Chem. Soc.* **2022**, *144*, 163−173.
(36) Li, M.; Xu, Y.; Pu, Z.; Xiong, T.; Huang, H.; Long, S.; Son, S.; Yu, L.; Singh, N.; Tong, Y.; Sessler, J. L.; Peng, X.; Kim, J. S. Photoredox

catalysis may be a general mechanism in photodynamic therapy. *Proc. Natl. Acad. Sci. U. S. A.* **2022**, *119*, No. e2210504119.
(37) Liu, M.; Luo, Y.; Yan, J.; Xiong, X.; Xing, X.; Kim, J. S.; Zou, T. Photoactivation of Boronic Acid Prodrugs via a Phenyl Radical Mechanism: Iridium(III) Anticancer Complex as an Example. *J. Am. Chem. Soc.* **2023**, *145*, 10082−10091.
(38) Kiyose, K.; Hanaoka, K.; Oushiki, D.; Nakamura, T.; Kajimura, M.; Suematsu, M.; Nishimatsu, H.; Yamane, T.; Terai, T.; Hirata, Y.; Nagano, T. Hypoxia-Sensitive Fluorescent Probes for in Vivo Real-Time Fluorescence Imaging of Acute Ischemia. *J. Am. Chem. Soc.* **2010**, *132*, 15846−15848.
(39) Patel, R. I.; Sharma, A.; Sharma, S.; Sharma, A. Visible light-mediated applications of methylene blue in organic synthesis. *Org. Chem. Front.* **2021**, *8*, 1694−1718.
(40) Pitre, S. P.; McTiernan, C. D.; Ismaili, H.; Scaiano, J. C. Mechanistic insights and kinetic analysis for the oxidative hydroxylation of arylboronic acids by visible light photoredox catalysis: a metal-free alternative. *J. Am. Chem. Soc.* **2013**, *135*, 13286−13289.
(41) Kalaitzakis, D.; Kouridaki, A.; Noutsias, D.; Montagnon, T.; Vassilikogiannakis, G. Methylene Blue as a Photosensitizer and Redox Agent: Synthesis of 5-Hydroxy-1H-pyrrol-2(5H)-ones from Furans. *Angew. Chem., Int. Ed.* **2015**, *54*, 6283−6287.
(42) Pitre, S. P.; McTiernan, C. D.; Scaiano, J. C. Library of Cationic Organic Dyes for Visible-Light-Driven Photoredox Transformations. *ACS Omega* **2016**, *1*, 66−76.
(43) Glaser, F.; Kerzig, C.; Wenger, O. S. Multi-Photon Excitation in Photoredox Catalysis: Concepts, Applications, Methods. *Angew. Chem., Int. Ed.* **2020**, *59*, 10266−10284.
(44) Liao, L.-L.; Song, L.; Yan, S.-S.; Ye, J.-H.; Yu, D.-G. Highly reductive photocatalytic systems in organic synthesis. *Trends Chem.* **2022**, *4*, 512−527.
(45) Ghosh, I.; Ghosh, T.; Bardagi, J. I.; König, B. Reduction of aryl halides by consecutive visible light-induced electron transfer processes. *Science* **2014**, *346*, 725−728.
(46) MacKenzie, I. A.; Wang, L.; Onuska, N. P. R.; Williams, O. F.; Begam, K.; Moran, A. M.; Dunietz, B. D.; Nicewicz, D. A. Discovery and characterization of an acridine radical photoreductant. *Nature* **2020**, *580*, 76−80.
(47) Zhao, Z.; Niu, F.; Li, P.; Wang, H.; Zhang, Z.; Meyer, G. J.; Hu, K. Visible Light Generation of a Microsecond Long-Lived Potent Reducing Agent. *J. Am. Chem. Soc.* **2022**, *144*, 7043−7047.
(48) Zeman, C. J. t.; Kim, S.; Zhang, F.; Schanze, K. S. Direct Observation of the Reduction of Aryl Halides by a Photoexcited Perylene Diimide Radical Anion. *J. Am. Chem. Soc.* **2020**, *142*, 2204−2207.
(49) Rieth, A. J.; Gonzalez, M. I.; Kudisch, B.; Nava, M.; Nocera, D. G. How Radical Are "Radical" Photocatalysts? A Closed-Shell Meisenheimer Complex Is Identified as a Super-Reducing Photoreagent. *J. Am. Chem. Soc.* **2021**, *143*, 14352−14359.
(50) Emmanuel, M. A.; Bender, S. G.; Bilodeau, C.; Carceller, J. M.; DeHovitz, J. S.; Fu, H.; Liu, Y.; Nicholls, B. T.; Ouyang, Y.; Page, C. G.; Qiao, T.; Raps, F. C.; Sorigue, D. R.; Sun, S. Z.; Turek-Herman, J.; Ye, Y.; Rivas-Souchet, A.; Cao, J.; Hyster, T. K. Photobiocatalytic Strategies for Organic Synthesis. *Chem. Rev.* **2023**, *123*, 5459−5520.
(51) Biegasiewicz, K. F.; Cooper, S. J.; Gao, X.; Oblinsky, D. G.; Kim, J. H.; Garfinkle, S. E.; Joyce, L. A.; Sandoval, B. A.; Scholes, G. D.; Hyster, T. K. Photoexcitation of flavoenzymes enables a stereoselective radical cyclization. *Science* **2019**, *364*, 1166−1169.
(52) Huang, X.; Wang, B.; Wang, Y.; Jiang, G.; Feng, J.; Zhao, H. Photoenzymatic enantioselective intermolecular radical hydroalkylation. *Nature* **2020**, *584*, 69−74.
(53) Mills, A.; Wang, J. Photobleaching of methylene blue sensitised by TiO2: an ambiguous system? *J. Photochem. Photobiol. A-Chem.* **1999**, *127*, 123−134.
(54) Faraji, M.; Farajtabar, A.; Gharib, F.; Ghasemnejad-Borsa, H. Deprotonation of salicylic acid and 5-nitrosalicylic acid in aqueous solutions of ethanol. *J. Serb. Chem. Soc.* **2011**, *76*, 1455−1463.
(55) Huang, S. D.; Shang, C.; Kang, P. L.; Zhang, X. J.; Liu, Z. P. LASP: Fast global potential energy surface exploration. *Wiley Interdiscip. Rev.-Comput. Mol. Sci.* **2019**, *9*, No. e1415.
(56) Huang, S.-D.; Shang, C.; Zhang, X.-J.; Liu, Z.-P. Material discovery by combining stochastic surface walking global optimization with a neural network. *Chem. Sci.* **2017**, *8*, 6327−6337.
(57) Wang, J.; Wang, X.; Fan, X.; Chen, P. R. Unleashing the Power of Bond Cleavage Chemistry in Living Systems. *ACS Cent. Sci.* **2021**, *7*, 929−943.
(58) Li, J.; Chen, P. R. Development and application of bond cleavage reactions in bioorthogonal chemistry. *Nat. Chem. Biol.* **2016**, *12*, 129−137.
(59) Bonnet, S. Ruthenium-Based Photoactivated Chemotherapy. *J. Am. Chem. Soc.* **2023**, *145*, 23397−23415.
(60) Bonnet, S. Why develop photoactivated chemotherapy? *Dalton Transactions* **2018**, *47*, 10330−10343.
(61) Lovejoy, K. S.; Lippard, S. J. Non-traditional platinum compounds for improved accumulation, oral bioavailability, and tumor targeting. *Dalton Transactions* **2009**, *47*, 10651−10659.
(62) van Rixel, V. H. S.; Ramu, V.; Auyeung, A. B.; Beztsinna, N.; Leger, D. Y.; Lameijer, L. N.; Hilt, S. T.; Le Dévédec, S. E.; Yildiz, T.; Betancourt, T.; Gildner, M. B.; Hudnall, T. W.; Sol, V.; Liagre, B.; Kornienko, A.; Bonnet, S. Photo-Uncaging of a Microtubule-Targeted Rigidin Analogue in Hypoxic Cancer Cells and in a Xenograft Mouse Model. *J. Am. Chem. Soc.* **2019**, *141*, 18444−18454.
(63) Zhang, L.; Wang, P.; Zhou, X.-Q.; Bretin, L.; Zeng, X.; Husiev, Y.; Polanco, E. A.; Zhao, G.; Wijaya, L. S.; Biver, T.; Le Dévédec, S. E.; Sun, W.; Bonnet, S. Cyclic Ruthenium-Peptide Conjugates as Integrin-Targeting Phototherapeutic Prodrugs for the Treatment of Brain Tumors. *J. Am. Chem. Soc.* **2023**, *145*, 14963−14980.

https://doi.org/10.1021/jacs.3c09837
J. Am. Chem. Soc. 2024, 146, 1364−1373